INTERNATIONAL JOURNAL OF AUTOMOTIVE AND MECHANICAL ENGINEERING
ISSN: 2229-8649 e-ISSN: 2180-1606
VOLUME 23, ISSUE 2, 2026, 13583 - 13600
DOI: https://doi.org/10.15282/ijame.23.2.2026.9.1028

RESEARCH ARTICLE

Crashworthiness behavior of additively manufactured PLA, nylon, and wood multicell tubes under axial and lateral quasi-static loading

Dony Hidayat[1,2], Jos Istiyanto[2], Danardono Agus Sumarsono[2], M Hafid[1]*, Riki Ardiansyah[1], Abian Nurrohmad[1], Redha Akbar Ramadhan[3], Aryandi Marta[1], Agus Harno Nurdin Syah[1], and Fadilah Hasim[1]

[1]Research Center for Aeronautics Technology, The National Research and Innovation Agency (BRIN), Bogor 16350, Indonesia
[2]Department of Mechanical Engineering, Faculty of Engineering, Universitas Indonesia, Depok 16424, Indonesia
[3]Department of Aerospace Engineering, Tohoku University, 6-6-01 Aramaki-Aza-Aoba, Aoba-ku, Sendai 980-8579, Japan

Abstract - Crashworthiness, which is defined as the ability of a structure to absorb impact energy through controlled, gradual deformation, is an important factor in the design of lightweight energy-absorbing structures. This study describes the crashworthiness behavior of multicell tubes with different internal cell geometries that have undergone quasi-static compression. Polylactic acid (PLA), nylon, and wood filaments were utilized in fused deposition modeling (FDM) to create thin-walled tubes with cross-shaped, equal-shaped, and strict inequality-shaped internal cell arrangements. The effects of material, internal geometry, build orientation, and loading orientation on the crashworthiness performance were analyzed experimentally. The cross-shaped design demonstrated the best crashworthiness performance among the examined configurations, especially for PLA specimens. The cross-shaped PLA tube produced the highest specific energy absorption (SEA) value of 10.75 J/g under axial compression, characterized by sequential folding deformation. Additionally, the specimens with a 90° orientation showed the most stable progressive collapse behavior and the greatest energy-absorption capacity. In comparison to PLA specimens made at a 90° build orientation, those made at a 45° and 0° build orientation absorbed 8.8% and 85.1% less energy, respectively. However, the wood specimens displayed the most severe brittle fracture, especially at lower build orientations. Under lateral compression, the cross-shaped arrangement offered the best compromise between structural weight and energy absorption (EA) capacity among the geometries examined. This result can be useful for the development of optimal energy-absorbing 3D printed thin-walled multicell structures, such as protective components and lightweight transportation structures.

Article History
Received : 3 June 2025
Revised : 17 May 2026
Accepted : 8 June 2026
Published : 30 June 2026

Keywords
Crashworthiness
Thin-walled structure
Additive manufacturing
Energy absorption
Axial and lateral loading
Quasi-static loading

1. Introduction

Thin-walled structures have been widely employed across various engineering sectors, including automotive [1, 2], rail [3], and aviation [4] because of their excellent energy dissipation capacity, low cost, and simple installation. Thin-walled tubes, such as crash boxes, side impact beams, and bumper structures, act as energy-absorbing components in automotive crash protection systems. The cross-sectional design significantly impacted how well a thin-walled structure absorbed energy [5]. Zhu et al. [6] conducted a comparative analysis of the crashworthiness of carbon fiber reinforced polymer (CFRP) tubes with various cross-sectional geometries. Their findings indicated that circular-section tubes have the greatest potential for energy absorption (EA), making them the most promising candidates for crashworthy structural applications. Furthermore, the aforementioned thin-walled structures, square [7-9], circular [10, 11], hexagonal [12, 13], hat-shaped [14], and multicell tubes [15-17], have been thoroughly studied in recent years using numerical modeling [18-20], experimental testing [21, 22], and theoretical analysis [23, 24]. For example, a parametric study has been conducted on cylindrical multicell columns [25]. The amount of energy absorbed is influenced differently by the wall's thickness and the number of cells, both radially and circumferentially. Most of the previous research has been on assessing the EA properties of multicell tubes made of metals and composite materials.

Thin-walled structures can be made using a variety of fabrication techniques, including extrusion, molding, welding, and composite lay-up procedures. However, the advancement of additive manufacturing (AM) technologies has been propelled by the increasing demand for intricate geometries, lightweight multicell setups, and quick design modification. AM has emerged as a practical technique for producing lightweight, geometrically complex energy-absorbing structures in recent years [26, 27]. One of the most significant developments in crashworthiness applications is the use of AM to design complex energy-absorbing structures with special capabilities [28]. Additionally, the aerospace, automotive, health, food, electronics, education, construction, architecture, and chemical industries have all made extensive use of AM technology, a rapidly expanding rapid prototyping approach [29, 30]. Fused deposition modeling (FDM), selective laser sintering (SLS), stereolithography (SLA), electron beam melting, laser melting, direct jetting, and photopolymer jetting are some of the categories into which AM can be divided [31]. FDM has become one of the most widely used methods due to its inexpensive cost, wide commercial availability, variety of materials, and ease of usage. Since Scott Crump created FDM technology in the 1980s [32], it has advanced quickly and is now widely accessible for usage in industry and research [33].

*CORRESPONDING AUTHOR | M Hafid | ✉ mhaf001@brin.go.id

The mechanical and crashworthiness performance of FDM-fabricated structures is strongly influenced by selecting filament material and printing conditions. There have been reports of polylactic acid (PLA) [34], polyamide (PA/nylon) [35], acrylonitrile butadiene styrene (ABS) [36], polyether ether ketone (PEEK) [37], and others [38]. These materials' unique mechanical and thermal characteristics have a big impact on thin-walled structures' crashworthiness, deformation behavior, and EA. PLA is frequently used due to its biodegradability, renewable origin, and attractive mechanical qualities [39], whereas nylon provides outstanding tensile strength, high toughness, and great thermal stability [40]. In addition, composite and reinforced filaments using carbon fiber, glass fiber, or wood particles have garnered increased attention recently due to their potential to enhance the mechanical performance of printed structures [41]. However, because of the layer-by-layer deposition process, FDM-printed structures exhibit anisotropic behavior in contrast to conventional materials, making their mechanical characteristics and failure mechanisms extremely sensitive to build orientation and interfacial bonding quality [42]. Therefore, understanding the characteristics of commercially available filament materials is critical for selecting the best material for designing thin-walled multicell structures made with FDM 3D printing.

The crashworthiness characteristics of polymeric materials produced through FDM techniques have been investigated in numerous studies [43, 44]. These studies have shown that the interaction between the metal and the FDM-printed multicell tube promotes the formation of additional deformation lobes and enhances EA. This hybrid configuration has significant potential to improve structural crashworthiness. The impact of printing parameters on energy EA capacity was the focus of early research. For instance, Tsouknidas et al. [45] investigated how printing parameters affect the EA performance of additively manufactured structures. They found that infill density has a major impact on EA capability, whereas layer height and infill pattern have comparatively less impact. Ma et al. [46] investigated the crashworthiness behavior of FDM–fabricated cubic structures with various infill patterns, infill densities, and material types under quasi-static compression. Their results showed that higher infill densities and honeycomb infill structures significantly enhanced the printed structures' ability to absorb energy. Wang et al. [47] examined the gradual collapse behavior of 3D-printed composite thin-walled structures and showed that bending and membrane deformation, together with matrix cracking, fiber–matrix debonding, and microfiber fracture, are deformation mechanisms. According to Idris et al. [48], under quasi-static compression, PLA-based FDM honeycomb sandwich structures outperformed thermoplastic polyurethane (TPU) and polyvinyl alcohol (PVA) based structures, achieving the maximum crashworthiness performance with a specific energy absorption (SEA) of 23.37 J/g. Furthermore, Kumar and Ma [49] examined the crashworthiness performance of lattice structures of thermoplastic polymer composites made by FDM with different geometric configurations under quasi-static compression. Their results showed that both the lattice geometry and the carbon-fiber-reinforced material significantly improved the SEA and crushing force efficiency (CFE) of the structures. Similarly, Alagesan et al. [50] analyzed the crashworthiness performance of biomimetic hexagonal multicell tubes made using FDM with polyethylene terephthalate glycol reinforced with carbon fiber (PETG-CF) filament. The silk spider web-inspired configuration demonstrated the highest total EA and SEA capacity among all investigated biomimetic designs under quasi-static axial compression. These experiments clearly show that in addition to material qualities, printing-induced structural features control the crashworthiness performance of additively built structures. The combined effects of internal multicell geometry, material type, build orientation, and loading orientation on the crashworthiness behavior of FDM-fabricated thin-walled tubes, particularly under both axial and lateral loading conditions, have received less attention despite the growing number of studies on AM crashworthy structures.

Although most previous studies have primarily focused on conventional geometries, single material systems, or individual printing parameters. Furthermore, this study investigates the crashworthiness behavior of multicell tubes undergoing quasi-static compression fabricated using FDM. PLA, nylon, and wood filaments were utilized to fabricate tubes with various internal multi-cell geometries, including cross-shaped, equal-shaped, and strict inequality-shaped configurations. The effects of filament material, internal geometry, build orientation, and loading orientation on the deformation behavior, EA capacity, and crushing stability were experimentally evaluated. The results of this work are expected to contribute to the development of lightweight energy-absorbing structures with improved crashworthiness performance and offer a deeper understanding of the crashworthiness features of FDM-printed multicell structures.

2. Materials and Methods

2.1 Materials and Prototyping

In this study, the filaments were made of PLA, nylon, and wood (Company X). The raw filament, which had a standard diameter of 1.75 mm, was fed inside a nozzle using a roller mechanism. Then, a 0.6-mm diameter nozzle was employed to extrude the molten filament. The material properties of the three filaments used in this study are shown in Table 1. A 3D printer creates PLA, nylon, and wood tubes one layer at a time in a height (z) direction. The specimens were fabricated with a layer height of 0.1 mm, a 100% infill density, and linear infill pattern. For the PLA and Wood tubes, the build plate temperature is kept at 60˚C, and the nozzle temperature is set to 210˚C. The printing platform and nozzle temperature for nylon tubes are maintained at 65˚C and 260˚C, respectively. The remaining 3D printer parameters are set as default values. A naming scheme is used for convenience. "P," "N," and "W" represent PLA, nylon, and wood tubes, respectively.

The printed multicell structure (Figure 1(a)) had three configurations inspired by mathematical symbols: cross (×), equals (=), and strict inequality (>). The build orientation of the multicell structure (shown in Figure 1(b)) was selected as 0°, 45°, and 90°. The tube wall thickness (t) and the structural walls of the multicell specimens were maintained at 1 mm, whereas the height (H) of all specimens was uniformly set to 50 mm. Each multicell structure had an outer diameter (D) of 25 mm. Figure 1(c) shows a representative model of the specimen. Table 2 summarizes the sectional areas of the various multicell configurations. In addition, all multicell structures featured a 45° chamfer on the outer top edge [51,

52]. This feature was intentionally introduced to prevent early localized failure at the tube edge during the early stages of crushing and promote progressive deformation in all multicell designs.

Table 1. Specification of each filament material

Properties	PLA	Nylon	Wood
Density (g/cm^3)	1.25	1.12	0.70
Tensile strength (MPa)	64	44	39
Elongation at Break (%)	4.17	164.88	5.97
Flexural strength (MPa)	40.5	54.2	23.7
Flexural modulus (GPa)	2.82	1.64	1.81
Izod impact strength (kJ/m^2)	2.15	4.44	1.97

Table 2. Section areas of the multicell structures

Specimens	Multicell ×	Multicell =	Multicell >
Section area (mm^2)	1.25	1.12	0.70

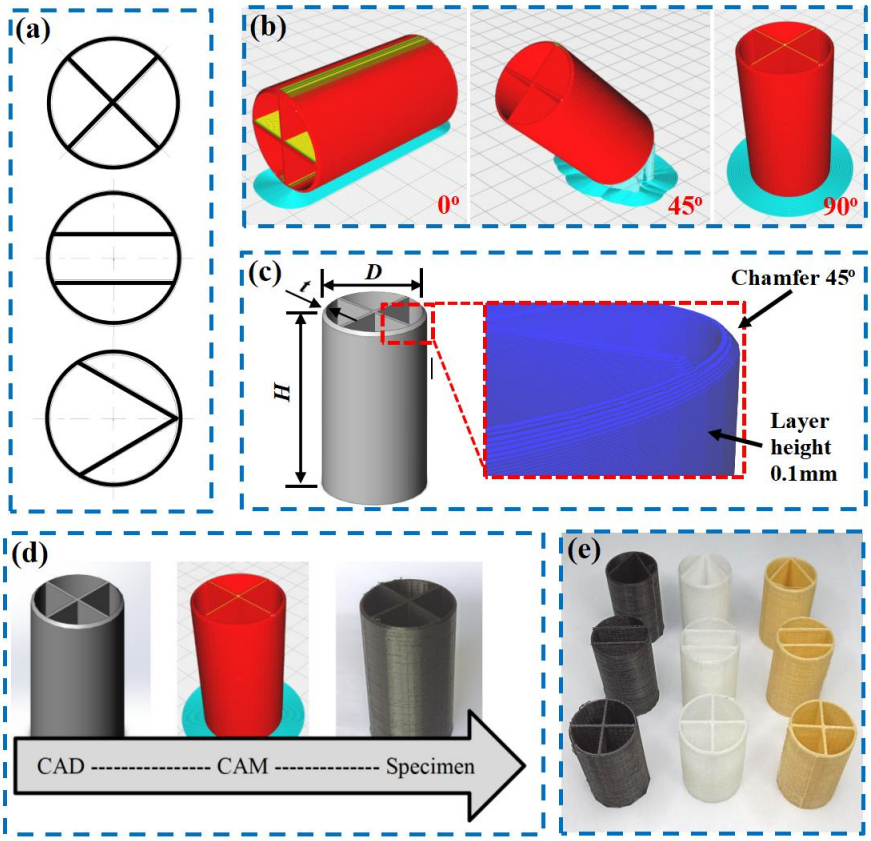

Figure 1. Specimen preparation: (a) multicell configuration design; (b) build orientation; (c) specimen dimension parameters; (d) process sequence; (e) printed multicell structures with different configurations and materials

Printing parameters were established using a 3D printing slicer software. Figure 1(d) depicts the preparation process flow of the samples. The multicell structure with cross configuration made by PLA was named P× for convenience. Meanwhile, configurations equal to and strict inequality are called P= and P>, respectively. The multicell with 90° build orientation made by PLA was named P90, while those with 45° and 0° directions were named P45 and P0, respectively. This name also applies to nylon (N90, N45, and N0) and wood (W90, W45, and W0) multicell tubes.

2.2 The Experimental Method

A universal testing machine with a loading capacity of 100 kN was used for experimental testing to apply axial and lateral quasi-static compressive forces. Numerous were considered when investigating the multicell tube's quasi-static testing. First, the experimental setup for quasi-static loading is simpler than a dynamic loading test. Second, under low-impact velocities, the structures exhibit EA responses and deformation modes that are strikingly comparable to those found under quasi-static loads. The testing was conducted at a crosshead speed of 5 mm/min [21, 53], with a maximum crushing displacement of 33 mm, or 2/3 of the initial total height [54, 55]. The crushing load and its corresponding displacement were recorded using the data acquisition system, and the entire test activity was recorded using a digital camera. Figures

2(a) and (b) depict the test setups for axial and lateral quasi-static compression, respectively. In addition, before and after conducting experimental quasi-static tests, microscopic analysis is used to examine the fabrication quality and fracture surfaces and to identify the corresponding failure mechanisms under different materials.

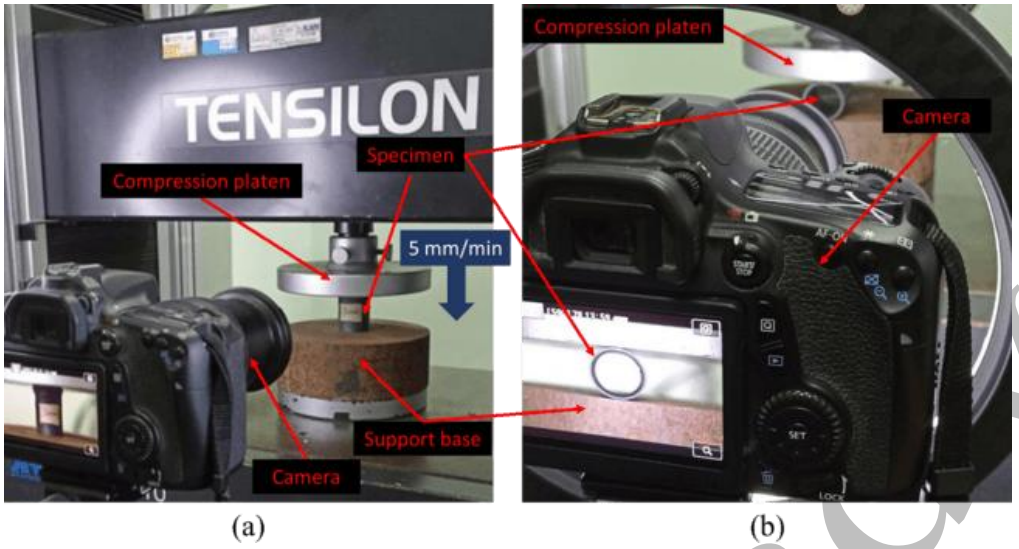

Figure 2. A quasi-static compression test experimental setup: (a) axial loading and (b) lateral loading

2.3 Characterization of Crashworthiness

Several distinct criteria are frequently used to assess crashworthiness performance, namely EA, mean crushing force (MCF), initial peak crushing force (IPCF), CFE, and SEA [56]. EA denotes the total energy dissipated throughout the crushing process and can be quantitatively determined by calculating the area beneath the force-displacement curve:

$$EA = \int_0^d F(x)dx \tag{1}$$

where *F(x)* represents the instantaneous crushing force and d denotes the displacement corresponding to the collapse distance. The MCF denotes the average force sustained throughout the crushing event and is defined as follows:

$$MCF = \frac{EA}{d} \tag{2}$$

CFE is used to describe how evenly the crushing force is applied. It can be calculated by dividing the MCF by the IPCF:

$$CFE = \frac{MCF}{IPCF} \tag{3}$$

SEA represents the energy absorbed by the structure's unit mass (m), and it is regarded as the most prevalent important indicator of the structure's capacity for absorbing energy, mathematically, as follows:

$$SEA = \frac{EA}{m} \tag{4}$$

3. Results and Discussions

3.1 The Effect of Material

The crushing processes of PLA, nylon, and wood tube under axial loading are shown in Figure 3. Following the IPCF, the thin-walled multicell tube gradually collapsed during compression. Throughout the entire compression phase, the plastic deformation proceeded in a continuous, stable, and uniform manner across all configurations, exhibiting a progressive collapse mode. PLA-made thin-walled multicell tubes showed the most regular progressive collapse behavior, characterized by sequential folding deformation and more EA during axial compression.

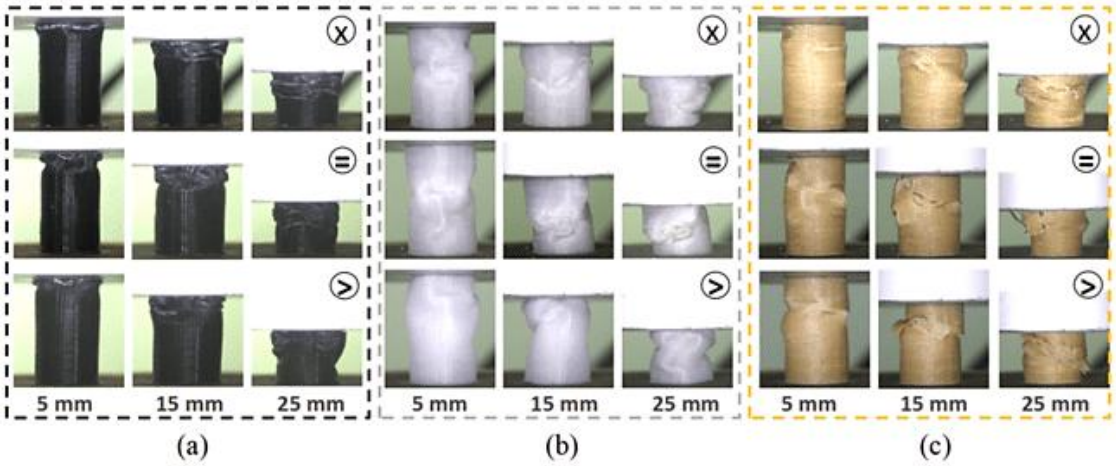

Figure 3. 3D printed thin-walled multicell structures collapse modes: (a) PLA; (b) nylon; and (c) wood

Figure 4 presents the force–displacement and energy absorption–displacement curves, which illustrate the thin-walled multicell structures' mechanical behavior and EA characteristics. All the specimens exhibited an IPCF, a force reduction, and a stable crushing area under quasi-static compression without significant fluctuations. The crushing response and EA characteristics of the multicell structures were strongly influenced by the type of material. The PLA specimens consistently showed the highest crushing loads and absorbed energy for all internal configurations among all the materials investigated. The PLA specimens typically showed smaller load reductions following the IPCF stage, suggesting improved structural integrity during progressive collapse. However, the nylon specimens showed the lowest crushing force of all the investigated materials, even though their deformation behavior seemed to be rather consistent and smooth throughout the compression process. The stiffness at early crushing, which is indicated by the slope in the pre-crushing area of the energy absorption–displacement curves, is another way to observe the impact of material type. Nylon specimens had the lowest slopes, indicating poor resistance to deformation, whereas PLA specimens showed the highest stiffness. Eventually, the wood specimens exhibited moderate stiffness and EA.

For all thin-walled multicell configurations, the IPCF for PLA and wood materials occurred within a displacement range of 2–4 mm, whereas the IPCF for nylon was only seen in N>. Among the three materials evaluated, the nylon multicell tube had the lowest EA. PLA has the highest EA capability among the three materials. The energy that the PLA materials can absorb in the three thin-walled multicell tubes ranges from 60 to 80 J. Wood and nylon can absorb energy between 20-30 J and 9-12 J, respectively.

The crashworthiness performance of tubes made of various materials is shown in Figure 5, and the relevant crashworthiness parameters derived from the axial compression tests are compiled in Table 3. The SEA and EA of the nylon tube are the lowest of the three tubes. The SEA of PLA and wood increased by 82% and 65%, respectively, compared with nylon. PLA had the highest EA (79.78 J) and SEA (10.75 J/g) values, as shown in Figure 5(a). The IPCF value of nylon was significantly lower than that of PLA and wood, but it had the highest CFE value (0.67). This is also shown in Figure 4, where the MCF of nylon was high and very similar to the IPCF. Figure 5(b) shows that the CFE values of PLA and wood were similar, but the IPCF of PLA was 59.1% higher than that of wood. As a result, the PLA thin-walled multicell tube displayed the highest EA stability over the entire plastic deformation process.

Scanning electron microscopy (SEM) was employed to characterize the morphology of the walls of FDM 3D-printed multicell tubes. Figure 6(a) shows a magnified view of the PLA tube wall. The printed sample has a layer thickness of about 99.5 µm, while the nylon and wood tubes have a layer thickness of 104 µm (Figure 6(b)) and 94.4 µm (Figure 6(c)), respectively. Micro and interlayer voids [57] appear in nylon tubes, and wormhole defects and interlayer voids appear in wood tubes. Interlayer voids Are typically smaller than worm-hole defects. The problem is most likely caused by a drop in layer thickness that increases the number of layers. As a result, uneven temperatures, unfavorable cooling, and poor melting quality [58].

Figure 7 illustrates the fracture patterns observed in PLA, nylon, and wood thin-walled multicell structures under axial quasi-static loading conditions. All materials exhibit plastic folding mode until the formation of the initial crack. A crack develops into the interlayer fracture in PLA and nylon, whereas wood fracture occurs, and large fragmentation is formed. The SEM image of the interlayer fracture between the PLA layers is shown in Figure 7(a). Along with horizontal bending deformation, the interlayer fracture was produced. The interlayer fracture started due to cracks that appeared when the bending force was greater than the adhesion force between the layers [47]. The interlayer fracture phenomenon also occurs in nylon (Figure 7(b)). The fracture pattern in multicell tubes made of PLA (Figure 7(a)) and wood (Figure 7(c)) is called ridge marking [59], which is an irregular micropattern on the fracture surface. More ridge marking on the fracture surface indicates greater energy dissipation upon collapse. A thin-walled multicell folding process, interlayer fracture, and intralayer fracture are the stages of the EA process. Interlayer fracture occurs when the crack plane runs parallel to the build plane, whereas intralayer fracture develops when the crack plane is perpendicular to the build plane [57].

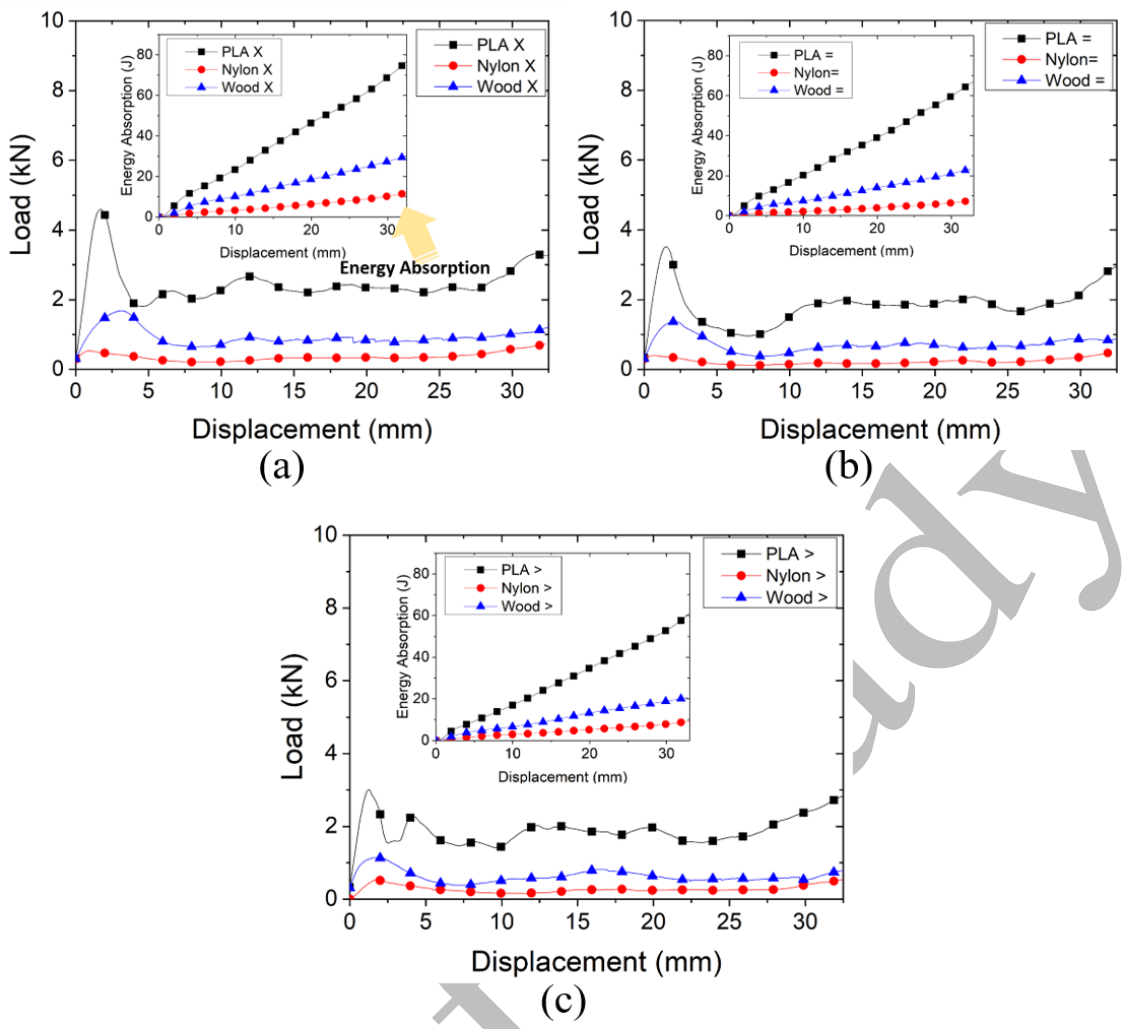

Figure 4. Force–displacement curves of multicell tubes of various materials and configurations: (a) cross-shaped; (b) equal-shaped; and (c) strict inequality-shaped

Table 3. Experimental result of quasi-static axial compression

Materials	Internal geometry	Build orientation	IPCF (kN)	MCF (kN)	CFE	EA (J)	SEA (J/g)
PLA	Single cell	90°	4.09±0.31	2.09±0.55	0.51±0.11	8.02±0.76	1.64±0.15
	×	90°	4.11±0.08	2.38±0.10	0.58±0.03	79.78±2.77	10.75±0.47
		45°	3.97±0.32	2.15±0.18	0.57±0.02	71.53±6.07	9.85±0.84
		0°	4.97±0.49	1.45±0.15	0.29±0.01	12.82±1.23	1.65±0.41
	=	90°	3.52±0.25	2.03±0.06	0.58±0.02	66.99±1.87	8.65±0.24
	>	90°	3.00±0.22	1.85±0.09	0.62±0.03	61.05±2.93	8.30±0.39
Nylon	×	90°	0.54±0.03	0.36±0.03	0.67±0.03	11.88±1.01	1.84±0.14
		45°	0.63±0.05	0.25±0.62	0.39±0.04	6.11±2.84	0.92±0.58
		0°	0.66±0.06	0.30±0.06	0.46±0.12	1.89±0.21	0.29±0.06
	=	90°	0.40±0.02	0.23±0.04	0.58±0.11	7.59±1.37	1.19±0.19
	>	90°	0.54±0.02	0.29±0.03	0.54±0.06	9.57±0.83	1.51±0.15
Wood	×	90°	1.68±0.04	0.93±0.10	0.55±0.06	30.69±3.32	5.26±0.53
		45°	1.16±0.52	0.68±0.29	0.59±0.03	1.28±0.71	0.22±0.12
		0°	1.82±0.19	0.81±0.04	0.45±0.06	2.46±0.67	0.42±0.11
	=	90°	1.38±0.29	0.72±0.08	0.52±0.10	23.76±2.58	4.10±0.54
	>	90°	1.14±0.18	0.63±0.05	0.55±0.07	20.79±1.49	3.86±0.36

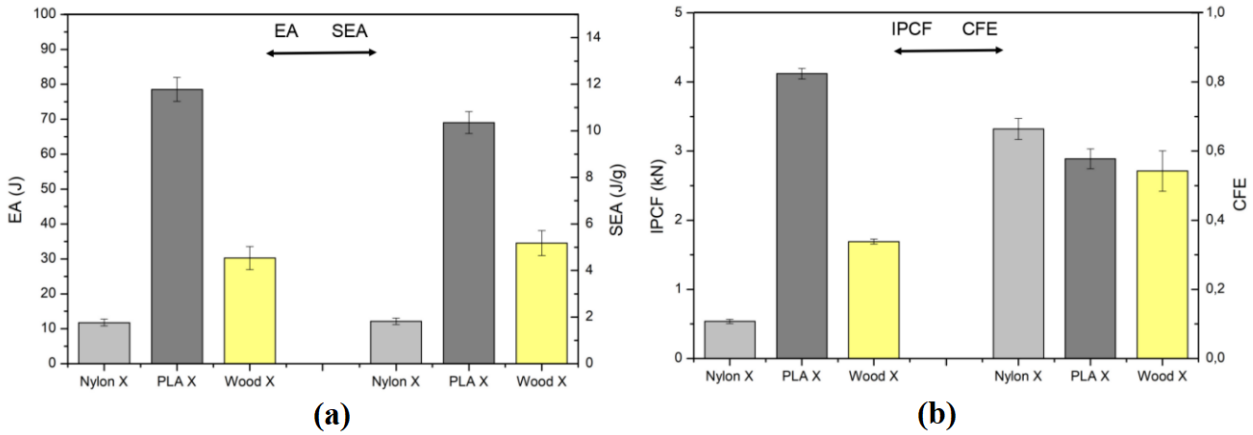

Figure 5. Effect of materials on crashworthiness properties: (a) EA and SEA and (b) IPCF and CFE

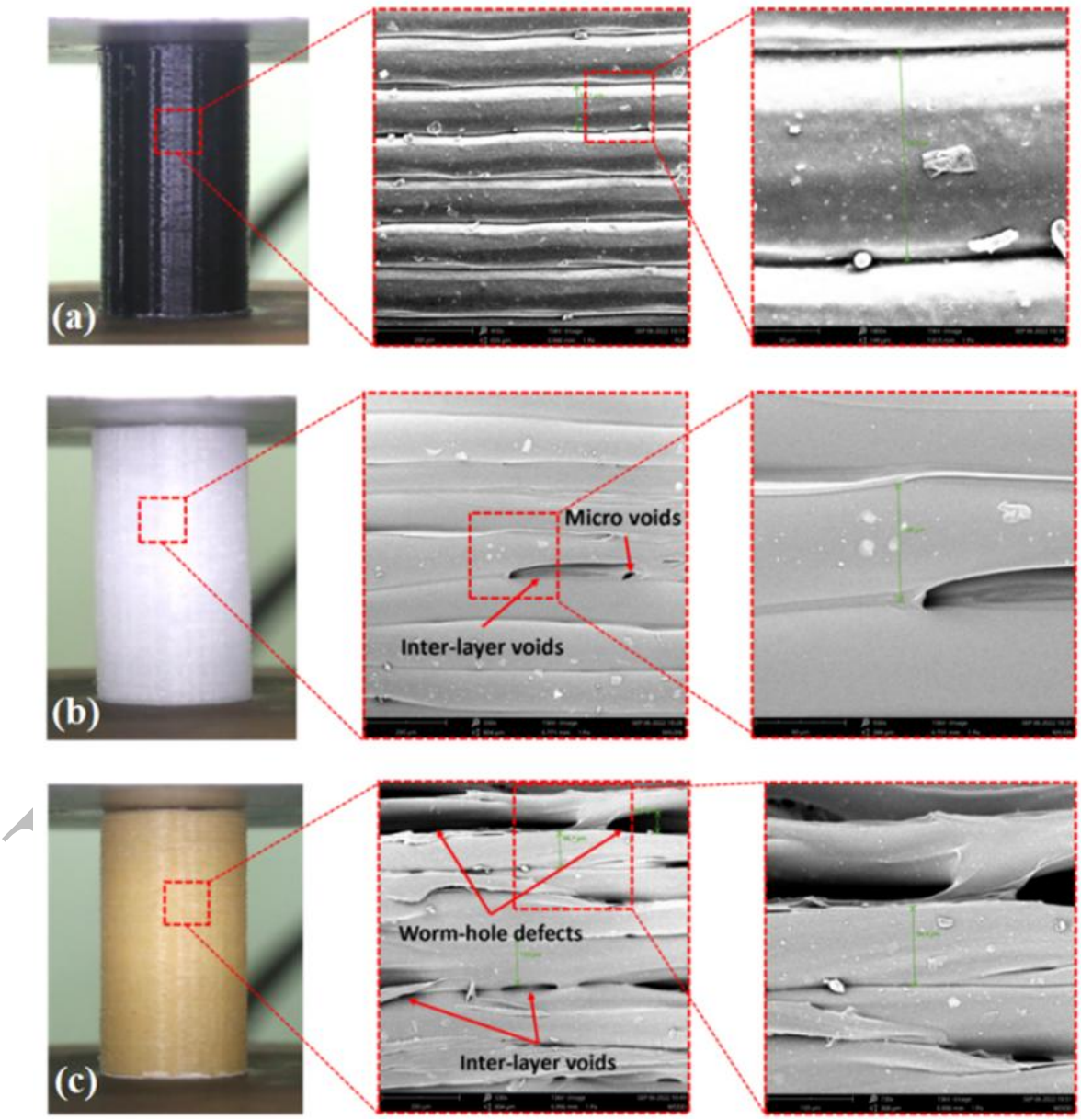

Figure 6. SEM images of the observed microstructure: (a) PLA; (b) nylon; and (c) wood

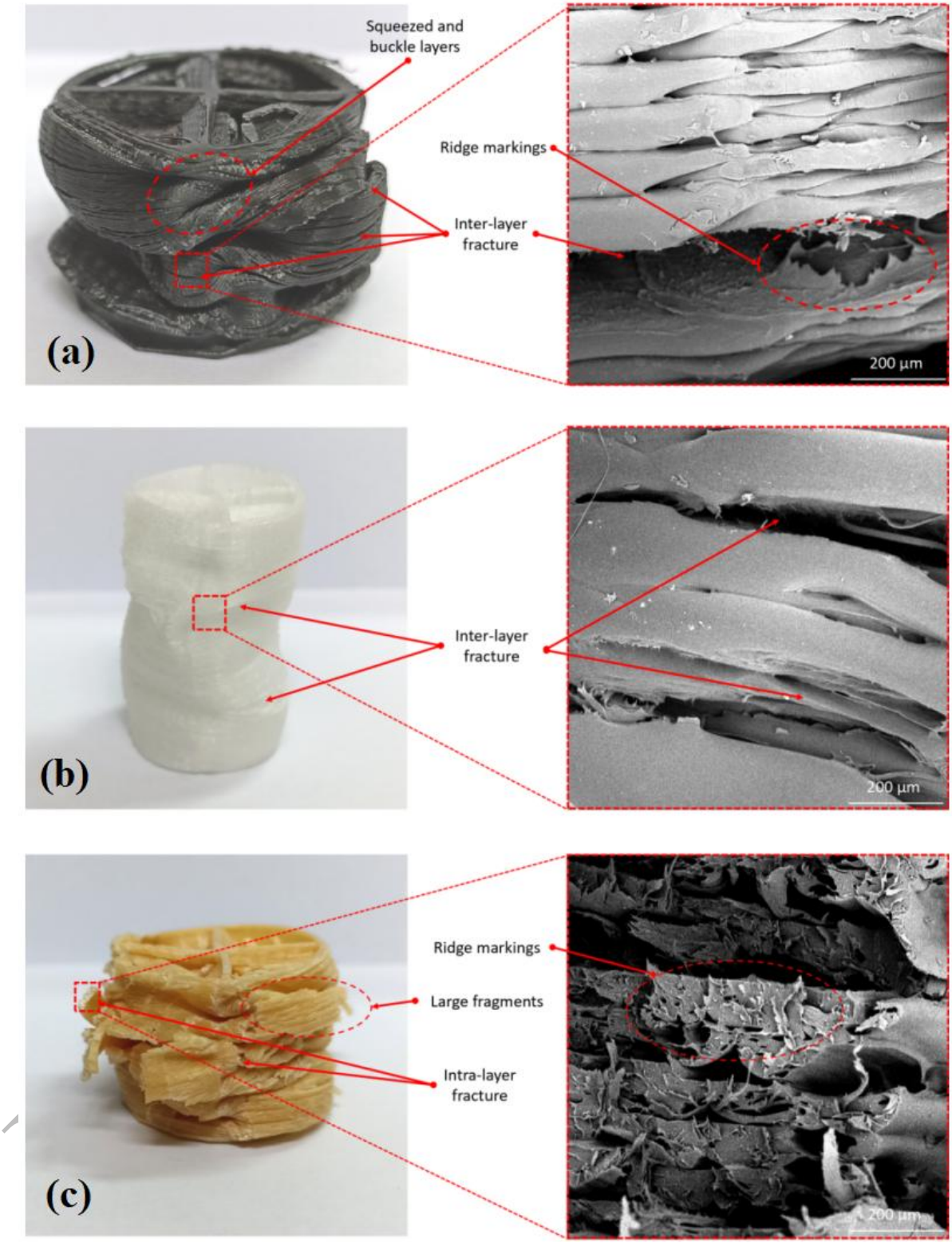

Figure 7. SEM images of the tube fracture surfaces of various materials: (a) PLA; (b) nylon; and (c) wood

3.2 Effect of Multicell Shape

Figures 8(a) and (b) illustrate the load-displacement curves and crushing processes of different shapes of multicell tubes, especially for PLA material. In the pre-crush stage, the crushing force immediately increased to its peak value, followed by an abrupt decrease to a lower value. These curves could be viewed as having similar patterns. The response curve can be categorized into three distinct stages: the pre-crushing stage, which is marked by the initiation of material failure; the post-crushing stage, which is characterized by the progressive propagation of damage throughout the specimen; and the compaction stage, which is characterized by the densification of the remaining debris [60]. Owing to the rise in yield strength and toughness, the IPCF of P× came out later. For P× and P=, after the IPCF, the biggest decline was observed. Compared with the other two structures, P> showed the lowest fluctuation and the highest CFE value.

Figure 9 shows that both the material type and multicell configuration significantly influence the SEA and CFE values of the multicell tubes. Among the investigated configurations, the cross-shaped configuration consistently exhibits the highest SEA values. For example, the W× and N× configurations showed greater SEA values than the other configurations within their respective material groups, while the P× configuration attained the maximum SEA value of 10.75 J/g. The cross-shaped internal design, which improves wall interaction during the crushing process, is responsible for this behavior. As a result, the progressive folding mechanism dissipates more plastic energy. However, for PLA and wood materials, the cross-shaped arrangement typically shows subtle CFE values, indicating larger IPCF values in comparison to the MCF during the crushing process. It's interesting to note that, of all the nylon-based structures, the N× configuration had the highest CFE value (0.67), which was also the highest CFE observed in this study. This result implies that nylon materials' cross-shaped design can encourage more stable deformation while preserving effective EA.

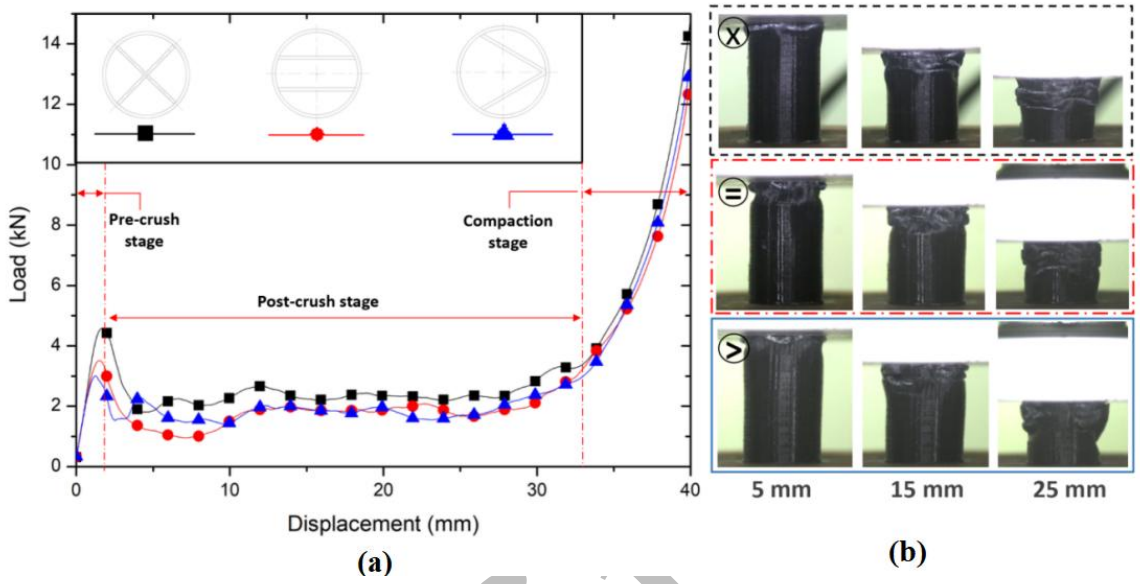

Figure 8. (a) Force–displacement curves and (b) crushing deformation sequences of multicell tubes with various cross-sectional geometries

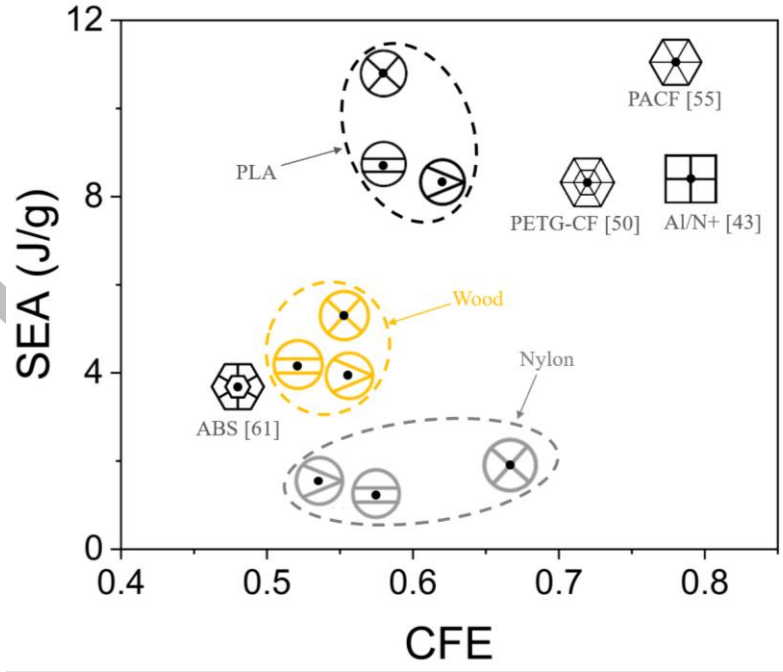

Figure 9. Effect of materials and multicell shape on crashworthiness characteristics: CFE and SEA

Conversely, for PLA and wood materials, the rigid inequality-shaped design typically yields larger CFE values than the other configurations. This trend is evident from the positions of the P> and W> configurations, which are located further to the right along the horizontal axis, indicating improved crushing-force stability during axial compression. The higher CFE values imply that the strict inequality-shaped configuration can more uniformly distribute the crushing load, thereby reducing the difference between IPCF and MCF, except in the case of nylon materials. However, the SEA values

of the strict inequality-shaped configurations are generally slightly lower than those of the cross-shaped configurations, indicating that the improved deformation stability does not necessarily correspond to the enhanced EA capacity. Meanwhile, the equal-shaped configuration demonstrates relatively balanced performance characteristics between SEA and CFE. In general, this configuration lies between the cross-shaped and strict inequality-shaped configurations in terms of both EA capacity and crushing efficiency. Nevertheless, the equal-shaped configuration consistently exhibits lower SEA and CFE values than the cross-shaped configuration for all investigated materials. Additionally, as shown on the graph's right side, the current findings were compared with previously documented energy-absorbing structures, specifically quadruple-cell square tubes fabricated from aluminum/nylon (Al/N+) hybrid materials [43], PETG-CF hexagonal tube inspired as a spider web [50], and hexagonal tubes filled with triangular cell made of short carbon-fiber-reinforced polyamide (PACF) [55]. These structures display relatively high CFE values (>0.7), indicating exceptional crushing stability. However, several combinations created in this study, especially P× and P>, continue to show competitive SEA performance. In addition, all PLA designs in this study performed better in terms of CFE and SEA than the hexagonal bi-tubular structure with wall-to-wall multicell manufactured of ABS [61]. Overall, the cross-shaped configuration is more effective in maximizing the EA capacity, whereas the strict inequality-shaped configuration provides better crushing-force stability. These results imply that, depending on whether the main goal is to maximize energy dissipation capacity or enhance deformation stability during impact loading, the internal arrangement can be customized to meet application requirements. Specifically, when compared to the other configurations under investigation, the cross-shaped structures exhibit better overall SEA performance.

A schematic of the folding feature lines for deformation in a single folding wavelength is presented in Figure 10. The P× specimen can be categorized as a Type-I deformation mode, in which the internal multicell members and the exterior tube wall fold in the same direction following axial crushing, according to Zhang's deformation mode categorization [10]. As the deformation pattern progressively and symmetrically develops along the tube axis in this manner, a stable folding mechanism is encouraged throughout the crushing operation. The folding feature lines formed during a single fold are represented by the dashed blue lines, which subsequently reverse direction in the next fold. Because the external wall and interior ribs work together to deform within the same folding wavelength, the P× design strengthens the bond between the tube wall and the multicell structure. The horizontal internal ribs in the P= arrangement, on the other hand, tend to direct the deformation along the transverse direction, exhibiting a somewhat simpler folding process that produces more uniform but less interactive folding patterns. The horizontal plastic hinge sections formed between the external wall and the internal parallel ribs are where the deformation is primarily concentrated. Consequently, the plastic's ability to disperse energy is reduced since there are fewer interacting folds and concentrated deformation zones than in the cross-shaped design. The P> configuration's inclined interior ribs display an asymmetric folding mechanism in which the deformation propagates preferentially toward one side of the cross-section. Because the inclined elements aid in the more gradual redistribution of the axial load throughout the structure, this process produces more stable progressive folding than the equal-shaped design. Even though the asymmetrical collapse mode shows comparatively stronger crushing stability, it also restricts the production of many simultaneous plastic hinges, resulting in lower SEA values as compared with the P× arrangement. The interaction between the internal members and the tube wall occurs primarily through the creation of inward folds along the tube walls, whereas the multicell structure primarily collapses inside the original cross-sectional boundary [62].

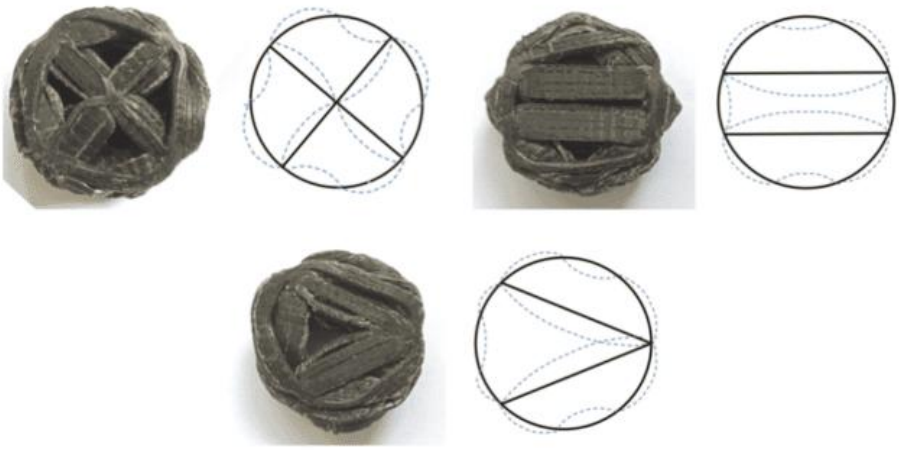

Figure 10. Deformation modes for multicell constituent elements

3.3 Effect of the Build Orientation

Thin-walled multicell tubes fabricated with 90°, 45°, and 0° build orientations were tested to characterize their crashworthiness behavior. Figure 11 shows the crushing behavior of thin-walled multicell tubes fabricated with different build orientations and materials under the same cross-shaped configuration. Every specimen exhibited steady progressive collapse behavior for the 90° construction orientation (Figure 11(a)). Because the deposited layers are positioned perpendicular to the loading direction in this arrangement, the compressive load is distributed more evenly throughout the tube structure. Under compressive loading, the materials' layers are squeezed out and compressed, and the structure

becomes compact. The squeezed layers are pulled away; this could be the result of the layer initially buckling and then breaking when the plastic deformation is too great or when it exceeds the material's fracture toughness [63]. At a 45° build orientation (Figure 11(b)), only the PLA and nylon tubes exhibited progressive collapse, whereas the wood tube fractured and disintegrated into large fragments. This behavior suggests that under oblique loading conditions, the interlayer cohesiveness of the wood-filled material was poorer and less resistant to shear-induced fracture propagation. Therefore, the structure failed before it could fully acquire steady progressive folding. All specimens showed interlayer fracture after axial crushing for the 0° build orientation (Figure 11(c)). The compressive load acts directly along the layer interfaces in this design because the deposited layers are oriented parallel to the loading direction. The main cause of failure was poor interfacial bonding between neighboring printed layers. Instead of forming progressive folds, the structures tended to separate layer by layer, which resulted in early delamination and unstable collapse behavior. The capacity of the tubes to withstand successive plastic deformation was greatly diminished by this interlayer fracture process, which also restricted their capacity to absorb energy.

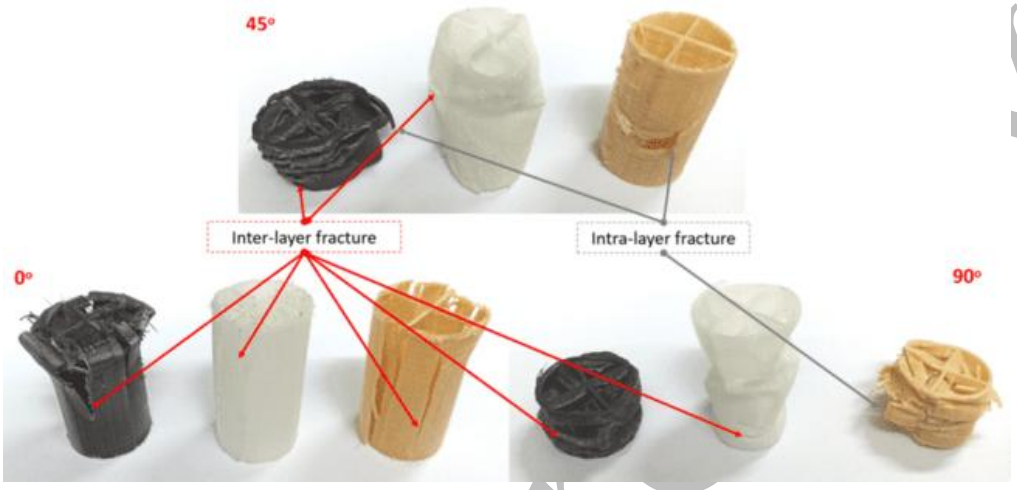

Figure 11. The effect of building orientation on the fracture mode

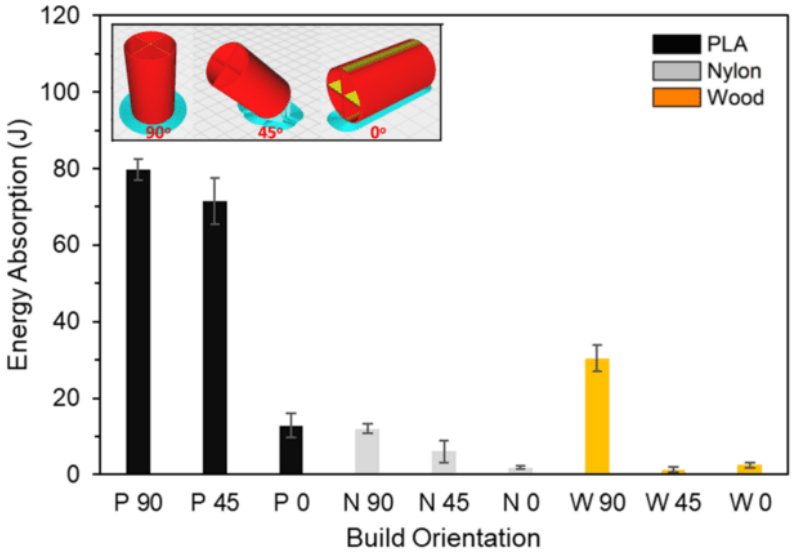

Figure 12. Comparison of the absorbed energy of the three-building orientation

The crushing behavior of FDM 3D printed thin-walled multicell tubes is significantly influenced by the build orientation. Simultaneously, EA reveals a prominent dependence on both building orientation and the type of materials. During the crushing process, a noticeable difference between the intralayer and interlayer fracture mechanisms can be observed. Intra-layer fracture became more prevalent in the 90° orientation, where the applied strain was mostly supported by the filament strands themselves, whereas inter-layer fracture was more common in the 0° build orientation due to debonding between adjacent deposited layers. The greater crushing stability observed in specimens made at higher construction orientations can be explained by this shift from interlayer to intralayer failure. Figure 12 depicts the crashworthiness characteristics of tubes made of various build orientations and materials. Among the investigated configurations, the specimens fabricated at a 90° build orientation consistently exhibited the highest EA capability. The P90 configuration, which reached approximately 79 J, had the maximum absorbed energy for the PLA specimens. In contrast, the absorbed energy dropped by 8.8% for the P45 specimen and by 85.1% for the P0 specimen. The very slight decrease in the 45° orientation indicates that even under inclined loading conditions, PLA materials retained sufficient

interlayer bonding strength for progressive collapse to proceed during crushing. The nylon multicell tubes showed a similar pattern. Among the nylon specimens, the N90 configuration exhibited the highest absorbed energy. The absorbed energies of N45 and N0 dropped by 38.9% and 86.4%, respectively. For the wood-filled specimens, the impact of the build orientation increased even more. While the absorbed energies of W45 and W0 dropped by 94.4% and 93.6%, respectively, the W90 configuration absorbed ~30 J of energy. In contrast to PLA and nylon, the wood-filled constructions showed severe brittle breakage and fragmentation at lower build orientations, especially at 45°. This behavior suggests that under combined compressive and shear stress conditions, the wood-filled material has low interlayer cohesion and limited fracture resistance. These findings are in line with earlier research published in the literature [64], which suggests that the build orientation affects the anisotropic mechanical properties produced by the layered manufacturing process in FDM 3D printing, primarily due to differences in the interfacial bonding between deposited layers.

3.4 Lateral Quasi-Static Loading

In addition to axial and oblique loading conditions, lateral loading may also be applied to structures. Figures 13 and 14 show the lateral deformation processes and compressive load-displacement curves of the multicell and single cell tubes, respectively. In contrast to the axial crushing of the same specimens, all multicell tubes have a low load-carrying capacity when subjected to lateral crushing [65]. The cross-sections of all the tubes instantly changed from round to elliptical as soon as the indenter made initial contact with the specimen.

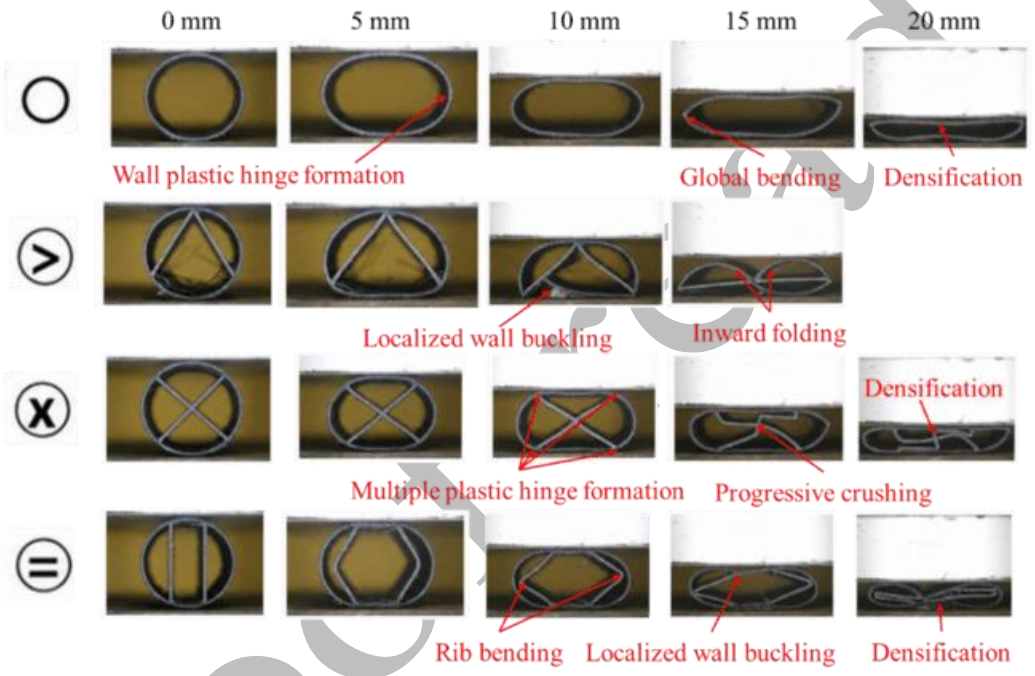

Figure 13. The deformation process of thin-walled multicell tubes subjected to lateral quasi-static loading

During lateral compression, the single-cell tube exhibited the most straightforward deformation mechanism. The crushing load increased to approximately 0.16 kN at a compression displacement of ~10 mm. Global structural bending with minimal internal interaction dominated the deformation, resulting in low compressive resistance and limited EA capability. During the crushing process, four plastic hinges were formed along the single-cell tube wall [66]. The multicell cross-shaped arrangement exhibited the most stable and progressive deformation behavior of all the structures examined. The crossed internal ribs continuously supported the outer wall during the crushing process, which led to a more even distribution of stress during lateral compression. With only slight local distortion, the cross-shaped arrangement structure maintained its geometric stability at a displacement of 5 mm. The IPCF value of the multicell cross-shaped tube is 0.97 kN at a displacement of 11 mm. Both the interior ribs and the outer wall experienced progressive folding simultaneously as the displacement increased to 10 and 15 mm, creating several plastic hinge regions. Instead of flattening completely, the structure retained a compact and interconnected collapse pattern even after a displacement of 20 mm.

The crushing load of the multicell strict inequality-shaped tube progressively increased until it reached an IPCF of 0.47 kN at a compression displacement of approximately 7.5 mm. Then, there was an abrupt drop in force, which was the beginning of the fracture at the bottom of the tube. Before the multicell tube totally collapsed, the crushing force steadily decreased as the compression process went on, reaching a displacement of 15 mm. In the meantime, an intermediate deformation response was displayed by the multicell arrangement with an equal shape. The IPCF in this configuration happened earlier, at a displacement of about 3 mm, but the parallel vertical ribs initially strengthened the lateral stiffness of the structure by limiting inward wall deformation. But as the compression grew, the internal ribs experienced global bending and eventually collapsed in the direction of the tube's center. Compared to the cross-shaped form, equal structure provided fewer contact points and easier folding patterns, which reduced the crushing resistance and EA capacity. However, because of the additional support provided by the internal ribs, the deformation remained more stable than that of the single cell structure.

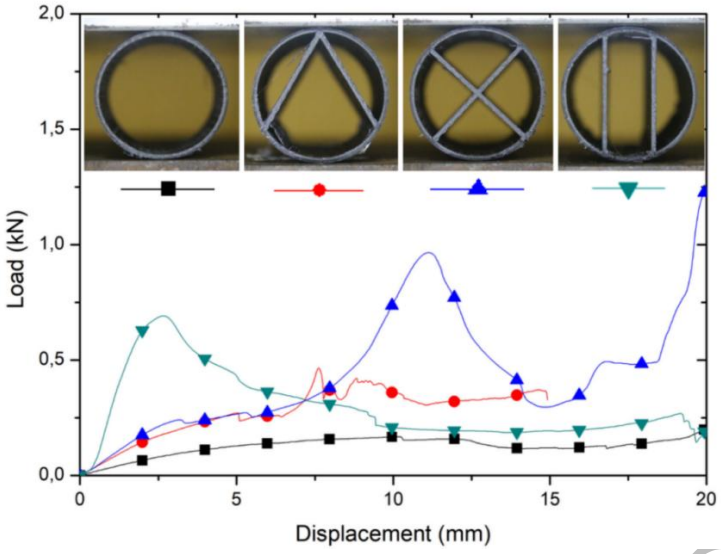

Figure 14. Load–Displacement curve of specimens subjected to lateral quasi-static loading

The quasi-static lateral compression test results for the examined thin-walled tubular structures are shown in Table 4. The multicell cross-shaped specimen demonstrated the best overall crashworthiness performance in accordance with the lateral compression crushing process. With IPCF, MCF, EA, and SEA values of 0.97 kN, 0.44 kN, 8.80 J, and 1.16 J/g, respectively, this setup attained the highest values. The cross-shaped internal reinforcement significantly enhanced the energy dissipation capabilities during lateral compression, as evidenced by the SEA value increasing by about 127% as compared to the single-cell tube. The greater connection between the internal ribs and outer wall, which encourages more stable deformation and produces more plastic hinge formations during crushing, is responsible for the improved performance. The efficacy of the suggested multicell designs is further demonstrated by a comparison with previously documented structures from the literature. Despite having a far lower mass, the multicell cross-shaped specimen attained a greater SEA value (1.16 J/g) than the single cell steel construction described in Ref. [65], which showed a SEA of 0.68 J/g. Furthermore, the composite single cell structure described in Ref. [66] absorbed a much higher total energy (137.45 J), but due to its much larger mass, the SEA value was only 0.30 J/g. These comparisons show that the suggested lightweight multicell designs provide better mass efficiency for EA applications, especially the multicell cross-shaped arrangement.

Overall, the findings show that adding internal multi-cell reinforcements significantly improves thin-walled tubes' lateral crashworthiness performance. The cross-shaped structure is a viable option for lightweight energy-absorbing applications because it offers the best balance between structural weight and energy absorption capacity among the geometries under investigation. Additionally, this study helps close the current knowledge gap about how the crashworthiness performance of FDM 3D-printed thin-walled multi-cell tubes is affected by material type, multi-cell geometry, build orientation, and loading orientation.

Table 4. Experimental result of quasi-static lateral compression

Specimens	IPCF (kN)	MCF (kN)	EA (J)	SEA (J/g)
Single cell	0.21±0.03	0.13±0.01	2.60±0.19	0.51±0.04
Multicell >	0.47±0.08	0.27±0.05	4.05±0.96	0.55±0.13
Multicell ×	0.97±0.14	0.44±0.10	8.80±0.23	1.16±0.27
Multicell =	0.69±0.03	0.30±0.01	6.00±0.08	0.78±0.01
Single cell steel [65]	-	0.51	9.31	0.68
Composite single cell [66]	1.97	0.85	137.45	0.30

3.5 The Effect of Loading Direction

The loading direction has a significant impact on the crashworthiness performance of additively manufactured thin-walled multicell tubes. Figure 15 displays the PLA multicell tubes' SEA and CFE values during axial and lateral quasi-static compression. The axial loading condition produced significantly higher SEA values (about 8–10.75 J/g) than the lateral loading condition (about 0.55–1.16 J/g) for all designs. This pattern implies that axial compression promotes more effective energy dissipation through stable progressive folding and improves the internal multicell walls' contribution during deformation.

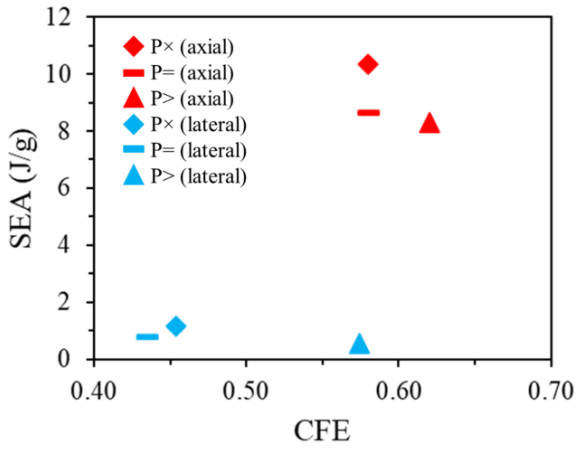

Figure 15. Impact of lateral and axial quasi-static pressure on the performance of CFE and SEA

The cross-shaped arrangement (P×) displayed the largest SEA under axial stress, whereas the strict inequality-shaped design (P>) demonstrated the maximum CFE, indicating superior crushing force stability. All specimens showed significantly lower SEA values because the deformation under lateral load was dominated by ovalization and localized bending rather than progressive folding. Nevertheless, with lateral compression, the cross-shaped arrangement remained to provide the best EA performance, while the rigid inequality-shaped configuration maintained the maximum CFE. Across all investigated geometries, the cross-shaped arrangement consistently demonstrated the highest crashworthiness behavior, and axial loading typically resulted in noticeably better EA performance than lateral loading.

4. Conclusions

The crashworthiness behavior of FDM-printed thin-walled multicell tubes under axial and lateral quasi-static loads was examined in this work. Several crashworthiness indicators, such as EA, MCF, IPCF, CFE, and SEA, were used to assess the effects of the filament material, multicell arrangement, build orientation, and loading direction. The following conclusions can be made considering the experimental findings:

- The material utilized has a significant impact on the printed tubes' crushing stability and EA capacity. Among the PLA, nylon, and wood specimens under axial quasi-static compression, the PLA multicell tubes exhibited the most reliable and progressive collapse behavior. PLA also demonstrated the best EA performance, with maximum EA and SEA values of 79.78 and 10.75 J, respectively. Nylon specimens exhibited the lowest EA capacity, whereas wood specimens tended to exhibit more severe fractures and fragmentation.
- The crashworthiness performance was significantly enhanced by the multicell structure. The cross-shaped multicell tube had the best EA capability among the examined cross-shaped, equal-shaped, and rigorous inequality-shaped arrangements. The cross-shaped interior wall structure offered a more efficient load transmission path and encouraged stable progressive deformation during crushing, as seen by the cross-shaped PLA specimen's maximum SEA of 10.75 J/g.
- The FDM-printed tubes' mechanical response was also significantly impacted by build orientation. When compared to the 45° and 0° orientations, the specimens printed with a 90° construction orientation showed the highest EA capacity. When compared to PLA with a 90° orientation, the absorbed energy of P45 and P0 for PLA specimens dropped by 8.8% and 85.1%, respectively. This outcome demonstrates that the layer arrangement used in the FDM technique has a significant impact on the energy dissipation capacity, failure mechanism, and crushing behavior of additively built thin-walled tubes.
- The loading direction has a major effect on the multicell tube crashworthiness response. Because progressive folding along the tube height was encouraged in the axial direction, axial quasi-static loading resulted in much greater SEA values than lateral quasi-static loading. By inducing cross-sectional ovalization, local buckling, plastic hinge formation, flattening, and compaction, lateral loading, on the other hand, decreased EA. The cross-shaped multicell structure performed best under lateral stress with IPCF = 0.97 kN, MCF = 0.44 kN, EA = 8.80 J, and SEA = 1.16 J/g.

Overall, the PLA cross-shaped multicell tube with a 90° build orientation demonstrated the most promising crashworthiness performance. Compared with the other investigated configurations, this configuration provided stable deformation, high EA, and superior SEA. Therefore, FDM-printed PLA multicell tubes, particularly those with cross-shaped internal walls, have strong potential for lightweight energy-absorbing applications in protective structures, transportation components, and unmanned aerial vehicle (UAV) related crashworthiness systems.

Acknowledgements

The authors acknowledge the facilities and technical support provided by the Aeronautics Laboratory and the Propellant and Quality Test Laboratory, The National Research and Innovation Agency (BRIN), Rumpin, through the E-Layanan Sains platform.

Funding
This work was supported by the project "Modular Design of Hybrid Composite Structure and 3D Printing for Impact-Resistant UAV Battery-Pack and Payload" No. 1/III.1/HK/2025 under the grant of Research Organization for Aeronautics and Space of The National Research and Innovation Agency (BRIN), Bogor, Indonesia.

Declaration of Competing Interest
The authors declare no conflicts of interest.

CRediT Authorship Contribution Statement
Dony Hidayat: Conceptualization, Methodology, Investigation, Visualization, Writing – original draft
Jos Istiyanto: Conceptualization, Methodology, Writing – review & editing
Danardono Agus Sumarsono: Conceptualization, Methodology, Supervision
M Hafid: Investigation, Writing – review & editing
Riki Ardiansyah: Data curation, Formal analysis, Project administration
Abian Nurrohmad: Formal analysis, Writing – review & editing
Redha Akbar Ramadhan: Data curation, Formal analysis, Investigation
Aryandi Marta: Data curation, Software
Agus Harno Nurdin Syah: Data curation
Fadilah Hasim: Writing – review & editing

Availability of Data and Materials
The datasets generated and/or analysed during the current study are available from the corresponding author on reasonable request.

Ethics Statement
This study did not involve human participants or animal subjects. Ethical approval was therefore not required for this research.

Generative Artificial Intelligence Declarations
The authors claim that artificially intelligent-assisted technologies, such as generative AI, were not used to generate content, ideas, or theories. We have just utilised AI to enhance readability and refine the language. This was used with extreme human control and oversight. The authors take full responsibility for reviewing and approving the content.

References
[1] Y. Zhang, G. Wang, Y. Zhang, et al., "Crashworthiness design of car threshold based on aluminium foam sandwich structure," *International Journal of Crashworthiness*, vol. 27, no. 4, pp. 1167-1178, 2022. https://doi.org/10.1080/13588265.2021.1914978
[2] N. Yang, P. Cao, T. Liu, J. Wang, D. Wang, "Crashworthiness optimisation of A-pillar in passenger car in rear-end collision with truck," *International Journal of Crashworthiness*, vol. 21, no. 6, pp. 507-520, 2016. https://doi.org/10.1080/13588265.2016.1192087
[3] T. Zhu, S. Xiao, C. Lei et al., "Rail vehicle crashworthiness based on collision energy management: An overview," *International Journal of Rail Transportation*, vol. 9, no. 2, pp. 101-131, 2021. https://doi.org/10.1080/23248378.2020.1777908
[4] H. Mou, J. Xie, Y. Liu, K. Cheng, Z. Feng, "Impact test and numerical simulation of typical sub-cargo fuselage section of civil aircraft," *Aerospace Science and Technology*, vol. 107, p. 106305, 2020. https://doi.org/10.1016/j.ast.2020.106305
[5] Z. Fan, G. Lu, K. Liu, "Quasi-static axial compression of thin-walled tubes with different cross-sectional shapes," *Engineering Structures*, vol. 55, pp. 80-89, 2013. https://doi.org/10.1016/j.engstruct.2011.09.020
[6] G. Zhu, G. Sun, G. Li, A. Cheng, Q. Li, "Modeling for CFRP structures subjected to quasi-static crushing," *Composite Structures*, vol. 184, pp. 41-55, 2018. https://doi.org/10.1016/j.compstruct.2017.09.001
[7] A.A. Nia, M. Parsapour, "Comparative analysis of energy absorption capacity of simple and multi-cell thin-walled tubes with triangular, square, hexagonal and octagonal sections," *Thin-Walled Structures*, vol. 74, pp. 155-165, 2014. https://doi.org/10.1016/j.tws.2013.10.005
[8] M. Hafid, J. Istiyanto, N. Nasruddin, "Multiobjective optimization of dimension and position of elliptical crush initiator on crashworthiness performance of square tube using response surface methodology," *Frontiers in Mechanical Engineering*, vol. 9, p. 1273447, 2023. https://doi.org/10.3389/fmech.2023.1273447
[9] F. Dionisius, J. Istiyanto, D.A. Sumarsono, G. Prayogo, A.S. Baskoro, M. Malawat, "Modeling of crashworthiness criteria based on variation of hole as crush initiator in thin-walled square," *International Journal of Automotive and Mechanical Engineering*, vol. 19, no. 1, pp. 9487-9497, 2022. https://doi.org/10.15282/ijame.19.1.2022.12.0731
[10] X. Zhang, H. Zhang, "Axial crushing of circular multi-cell columns," *International Journal of Impact Engineering*, vol. 65, pp. 110-125, 2014. https://doi.org/10.1016/j.ijimpeng.2013.12.002

[11] D. Hidayat, R. Ardiansyah, A. Nurrohmad, R.A. Ramadhan, J. Istiyanto, F. Karina, et al., "Experimental study on crashworthiness characteristics of composite hybrid tube utilise axial quasi-static crushing test," in *AIP Conference Proceedings*, vol 2941, p. 020012, 2023. https://doi.org/10.1063/5.0181353
[12] N. Qiu, Y. Gao, J. Fang, Z. Feng, G. Sun, Q. Li, "Crashworthiness analysis and design of multi-cell hexagonal columns under multiple loading cases," *Finite Elements in Analysis and Design*, vol. 104, pp. 89-101, 2015. https://doi.org/10.1016/j.finel.2015.06.004
[13] D. Hidayat, J. Istiyanto, D.A. Sumarsono, F. Kurniawan, R. Ardiansyah, F.A. Wandono, et al., "Investigation on the crashworthiness performance of thin-walled multi-cell PLA 3D-printed tubes: A multi-parameter analysis," *Designs*, vol. 7, no. 5, p. 108, 2023. https://doi.org/10.3390/designs7050108
[14] Z. Du, L. Duan, A. Cheng, B. Wei, G. Zhang, "Theoretical prediction and analysis of hybrid material hat-shaped tubes with strengthened corner structures under quasi-static axial loading," *Engineering Structures*, vol. 230, p. 111699, 2021. https://doi.org/10.1016/j.engstruct.2020.111699
[15] A. Jusuf, T. Dirgantara, L. Gunawan, I.S. Putra, "Crashworthiness analysis of multi-cell prismatic structures," *International Journal of Impact Engineering*, vol. 78, pp. 34-50, 2015. https://doi.org/10.1016/j.ijimpeng.2014.11.011
[16] R. Ardiansyah, F.K. Indriani, D. Hidayat, A. Tjahjono, A. Nurrohmad, A. Marta, "Crashworthiness performance study of 3D-printed multi-cell tubes hybridized with aluminum under axial quasi-static testing," *Automotive Experiences*, vol. 7, no. 3, pp. 567-578, 2024. https://doi.org/10.31603/ae.12247
[17] M. Hafid, A. Nurrohmad, D. Hidayat, R. Ardiansyah, A. Marta, C.A. Rosalia, et al., "Low-velocity impact response of novel hierarchical hexagonal multicell structures," *International Journal of Lightweight Materials and Manufacture*, vol. 9, no. 1, pp. 20-36, 2026. https://doi.org/10.1016/j.ijlmm.2025.07.008
[18] M. Davoudi, C. Kim, "Evaluation of the axial crashworthiness of thin-walled structures with various and combined cross sections," *Journal of Mechanical Science and Technology*, vol. 32, no. 9, pp. 4271-4281, 2018. https://doi.org/10.1007/s12206-018-0825-1
[19] Z. Xie, Z. Zhao, C. Li, "Bending crashworthiness of thin-walled square tubes with multi-cell and double-tube cross-sections," *Journal of Mechanical Science and Technology*, vol. 35, pp. 4815-4823, 2021. https://doi.org/10.1007/s12206-021-1001-6
[20] X.Y. Ang, C. Hassan, S. Soh, E. Olugu, N. Abdullah, L. Yu, et al., "Evaluation of automotive bio-composites crash box performance," *International Journal of Automotive and Mechanical Engineering*, vol. 20, no. 4, pp. 10943-10952, 2023. https://doi.org/10.15282/ijame.20.4.2023.11.0846
[21] D. Hidayat, A. Nurrohmad, A. Nugroho, L.R. Isna, "Experimental investigation on crashworthiness characteristics of e-glass–lycal composite tube and local product aluminum tube using quasi-static crushing test," in *AIP Conference Proceedings*, 2020, p. 040007. https://doi.org/10.1063/5.0002313
[22] S. Wang, M. Zhang, Y. Wang, Z. Huang, Y. Fang, "Experimental studies on quasi-static axial crushing of additively-manufactured PLA random honeycomb-filled double circular tubes," *Composite Structures*, vol. 261, p. 113553, 2021. https://doi.org/10.1016/j.compstruct.2021.113553
[23] W. Abramowicz, N. Jones, "Dynamic axial crushing of circular tubes," *International Journal of Impact Engineering*, vol. 2, no. 3, pp. 263-281, 1984. https://doi.org/10.1016/0734-743X(84)90010-1
[24] T. Wierzbicki, S.U. Bhat, W. Abramowicz, D. Brodkin, "Alexander revisited—a two folding elements model of progressive crushing of tubes," *International Journal of Solids and Structures*, vol. 29, no. 24, pp. 3269-3288, 1992.
[25] Z. Tang, S. Liu, Z. Zhang, "Analysis of energy absorption characteristics of cylindrical multi-cell columns," *Thin-Walled Structures*, vol. 62, pp. 75-84, 2013. https://doi.org/10.1016/0020-7683(92)90040-Z
[26] A. Meram, B. Sözen, "Experimental investigation on the effect of printing parameters on the impact response of thin-walled tubes produced by additive manufacturing method," *International Journal of Crashworthiness*, vol. 28, no. 1, pp. 32-45, 2023. https://doi.org/10.1080/13588265.2022.2045824
[27] F. Habib, P. Iovenitti, S. Masood, M. Nikzad, "In-plane energy absorption evaluation of 3D printed polymeric honeycombs," *Virtual and Physical Prototyping*, vol. 12, no. 2, pp. 117-131, 2017. https://doi.org/10.1080/17452759.2017.1291354
[28] C.W. Isaac, F. Duddeck, "Current trends in additively manufactured (3D printed) energy absorbing structures for crashworthiness application–a review," *Virtual and Physical Prototyping*, vol. 17, no. 4, pp. 1058-1101, 2022. https://doi.org/10.1080/17452759.2022.2074698
[29] N. Shahrubudin, T.C. Lee, R. Ramlan, "An overview on 3D printing technology: Technological, materials, and applications," *Procedia manufacturing*, vol. 35, pp. 1286-1296, 2019. https://doi.org/10.1016/j.promfg.2019.06.089
[30] A. Albar, M. Chougan, M.J. Al-Kheetan, M.R. Swash, S.H. Ghaffar, "Effective extrusion-based 3D printing system design for cementitious-based materials," *Results in engineering*, vol. 6, p. 100135, 2020. https://doi.org/10.1016/j.rineng.2020.100135
[31] R. Amin, S. Knowlton, A. Hart, B. Yenilmez, F. Ghaderinezhad, S. Katebifar, et al., "3D-printed microfluidic devices," *Biofabrication*, vol. 8, no. 2, p. 022001, 2016. https://doi.org/10.1088/1758-5090/8/2/022001
[32] M. Srivastava, S. Rathee, "Optimisation of FDM process parameters by Taguchi method for imparting customised properties to components," *Virtual and Physical Prototyping*, vol. 13, no. 3, pp. 203-210, 2018. https://doi.org/10.1080/17452759.2018.1440722

[33] T.N.A.T. Rahim, A.M. Abdullah, H. Md Akil, "Recent developments in fused deposition modeling-based 3D printing of polymers and their composites," *Polymer Reviews*, vol. 59, no. 4, pp. 589-624, 2019. https://doi.org/10.1080/15583724.2019.1597883
[34] O. Ezeh, L. Susmel, "On the notch fatigue strength of additively manufactured polylactide (PLA)," *International Journal of Fatigue*, vol. 136, p. 105583, 2020. https://doi.org/10.1016/j.ijfatigue.2020.105583
[35] Y. Peng, Y. Wu, S. Li, K. Wang, S. Yao, Z. Liu, et al., "Tailorable rigidity and energy-absorption capability of 3D printed continuous carbon fiber reinforced polyamide composites," *Composites Science and Technology*, vol. 199, p. 108337, 2020. https://doi.org/10.1016/j.compscitech.2020.108337
[36] C.T. Ng, L. Susmel, "Notch static strength of additively manufactured acrylonitrile butadiene styrene (ABS)," *Additive Manufacturing*, vol. 34, p. 101212, 2020. https://doi.org/10.1016/j.addma.2020.101212
[37] M.F. Arif, H. Alhashmi, K. Varadarajan, J.H. Koo, A. Hart, S. Kumar, "Multifunctional performance of carbon nanotubes and graphene nanoplatelets reinforced PEEK composites enabled via FFF additive manufacturing," *Composites Part B: Engineering*, vol. 184, p. 107625, 2020. https://doi.org/10.1016/j.compositesb.2019.107625
[38] E.J. Hunt, C. Zhang, N. Anzalone, J.M. Pearce, "Polymer recycling codes for distributed manufacturing with 3-D printers," *Resources, Conservation and Recycling*, vol. 97, pp. 24-30, 2015. https://doi.org/10.1016/j.resconrec.2015.02.004
[39] D. Garlotta, "A literature review of poly(lactic acid)," *Journal of Polymers and the Environment*, vol. 9, no. 2, pp. 63-84, 2001. https://doi.org/10.1023/A:1020200822435
[40] N.G. Karsli, A. Aytac, "Tensile and thermomechanical properties of short carbon fiber reinforced polyamide 6 composites," *Composites Part B: Engineering*, vol. 51, pp. 270-275, 2013. https://doi.org/10.1016/j.compositesb.2013.03.023
[41] M.S. Saharudin, J. Hajnys, T. Kozior, D. Gogolewski, P. Zmarzły, "Quality of surface texture and mechanical properties of PLA and PA-based material reinforced with carbon fibers manufactured by FDM and CFF 3D printing technologies," *Polymers*, vol. 13, no. 11, p. 1671, 2021. https://doi.org/10.3390/polym13111671
[42] A. Nurrohmad, F.A. Wandono, A.R. Nuranto, M. Hafid, T.K. Wardana, K. Abdurohman, et al., "Rapid prototyping assisted optimization and experimental three point bending evaluation of spreader bar structure," *International Journal of Lightweight Materials and Manufacture*, vol. 9, no. 1, pp. 47-59, 2026. https://doi.org/10.1016/j.ijlmm.2025.08.004
[43] X. Fu, X. Zhang, Z. Huang, "Axial crushing of Nylon and Al/Nylon hybrid tubes by FDM 3D printing," *Composite Structures*, vol. 256, p. 113055, 2021. https://doi.org/10.1016/j.compstruct.2020.113055
[44] D. Hidayat, J. Istiyanto, J.D. Nabilah, R. Ardiansyah, S.A. Saptari, F. Kurniawan, et al., "Experimental investigation on axial quasi-static crushing of Al/PLA hybrid tubes," *Journal of Physics: Conference Series*, vol. 2551, p. 012008, 2023. https://doi.org/10.1088/1742-6596/2551/1/012008
[45] A. Tsouknidas, M. Pantazopoulos, I. Katsoulis, D. Fasnakis, S. Maropoulos, N. Michailidis, "Impact absorption capacity of 3D-printed components fabricated by fused deposition modelling," *Materials & Design*, vol. 102, pp. 41-44, 2016. https://doi.org/10.1016/j.matdes.2016.03.154
[46] Q. Ma, M. Rejab, A.P. Kumar, H. Fu, N.M. Kumar, J. Tang, "Effect of infill pattern, density and material type of 3D printed cubic structure under quasi-static loading," *Proceedings of the Institution of Mechanical Engineers, Part C: Journal of Mechanical Engineering Science*, vol. 235, no. 19, 4254-4272, 2021. https://doi.org/10.1177/0954406220971667
[47] J. Wang, Y. Liu, K. Wang, S. Yao, Y. Peng, Y. Rao, et al., "Progressive collapse behaviors and mechanisms of 3D printed thin-walled composite structures under multi-conditional loading," *Thin-Walled Structures*, vol. 171, p. 108810, 2022. https://doi.org/10.1016/j.tws.2021.108810
[48] M. Idris, Q. Ma, N.A. Aziz, A. Mohammed, B. Zhang, M. Rejab, "3D-printed honeycomb sandwich structures: Mechanical characterisation of biocomposite materials," in *Biocomposites for Lightweight Sandwich Structures*: CRC Press, 2024, pp. 31-45. https://doi.org/10.1201/9781003368977
[49] P. Kumar A, Q. Ma, "Evaluation of energy absorption enhancement of additively manufactured polymer composite lattice structures," *Functional Composites and Structures*, vol. 5, no. 1, 015005, 2023. https://doi.org/10.1088/2631-6331/acc0d0
[50] P.K. Alagesan, G. Krishnan, S.K. Sahu, A. Kumaresan Gladys, S. Subbarayan, Q. Ma, "Crashworthiness performance of 3D printed thermoplastic polymer composite hexagonal multi-cellular tubes: A biomimetic approach for enhanced energy absorption," *Journal of Thermoplastic Composite Materials*, vol. 39, no. 3, 1261-1290, 2026. https://doi.org/10.1177/08927057251368873
[51] J. Xu, Y. Ma, Q. Zhang, T. Sugahara, Y. Yang, H. Hamada, "Crashworthiness of carbon fiber hybrid composite tubes molded by filament winding," *Composite Structures*, vol. 139, pp. 130-140, 2016. https://doi.org/10.1016/j.compstruct.2015.11.053
[52] M. Haolei, X. Jiang, Z. Jun, F. Zhenyu, "Experimental researches on failure and energy absorption of composite laminated thin-walled structures," *Journal of Composite Materials*, vol. 54, no. 27, pp. 4253-4268, 2020. https://doi.org/10.1177/0021998320928135
[53] S. Tabacu, C. Ducu, "Experimental testing and numerical analysis of FDM multi-cell inserts and hybrid structures," *Thin-Walled Structures*, vol. 129, pp. 197-212, 2018. https://doi.org/10.1016/j.tws.2018.04.009

[54] G. Sun, S. Li, Q. Liu, G. Li, Q. Li, "Experimental study on crashworthiness of empty/aluminum foam/honeycomb-filled CFRP tubes," *Composite Structures*, vol. 152, pp. 969-993, 2016. https://doi.org/10.1016/j.compstruct.2016.06.019
[55] K. Wang, Y. Liu, J. Wang, J. Xiang, S. Yao, Y. Peng, "On crashworthiness behaviors of 3D printed multi-cell filled thin-walled structures," *Engineering Structures*, vol. 254, p. 113907, 2022. https://doi.org/10.1016/j.engstruct.2022.113907
[56] G. Zhu, J. Liao, G. Sun, Q. Li, "Comparative study on metal/CFRP hybrid structures under static and dynamic loading," *International Journal of Impact Engineering*, vol. 141, p. 103509, 2020. https://doi.org/10.1016/j.ijimpeng.2020.103509
[57] Z. Zhang, D. Yavas, Q. Liu, D. Wu, "Effect of build orientation and raster pattern on the fracture behavior of carbon fiber reinforced polymer composites fabricated by additive manufacturing," *Additive Manufacturing*, vol. 47, p. 102204, 2021. https://doi.org/10.1016/j.addma.2021.102204
[58] O.A. Mohamed, S.H. Masood, J.L. Bhowmik, "Characterization and dynamic mechanical analysis of PC-ABS material processed by fused deposition modelling: An investigation through I-optimal response surface methodology," *Measurement*, vol. 107, pp. 128-141, 2017. https://doi.org/10.1016/j.measurement.2017.05.019
[59] M.R. Ayatollahi, A. Nabavi-Kivi, B. Bahrami, M. Yazid Yahya, M.R. Khosravani, "The influence of in-plane raster angle on tensile and fracture strengths of 3D-printed PLA specimens," *Engineering Fracture Mechanics*, vol. 237, p. 107225, 2020. https://doi.org/10.1016/j.engfracmech.2020.107225
[60] K.S. Raju, J.S. Tomblin, "Energy absorption characteristics of stitched composite sandwich panels," *Journal of Composite Materials*, vol. 33, no. 8, pp. 712-728, 1999. https://doi.org/10.1177/002199839903300804
[61] M. Tunay, A. Bardakci, "A study of crashworthiness performance in thin-walled multi-cell tubes 3D-printed from different polymers," *Journal of Applied Polymer Science*, vol. 141, no. 48, p. e56287, 2024. https://doi.org/10.1002/app.56287
[62] S. Wang, M. Zhang, W. Pei, F. Yu, Y. Jiang, "Energy-absorbing mechanism and crashworthiness performance of thin-walled tubes diagonally filled with rib-reinforced foam blocks under axial crushing," *Composite Structures*, vol. 299, p. 116149, 2022. https://doi.org/10.1016/j.compstruct.2022.116149
[63] M.S. Uddin, M.F.R. Sidek, M.A. Faizal, R. Ghomashchi, A. Pramanik, "Evaluating mechanical properties and failure mechanisms of fused deposition modeling acrylonitrile butadiene styrene parts," *Journal of Manufacturing Science and Engineering*, vol. 139, no. 8, p. 081018, 2017. https://doi.org/10.1115/1.4036713
[64] K.M. Ashtankar, A.M. Kuthe, B.S. Rathour, "Effect of build orientation on mechanical properties of rapid prototyping (fused deposition modelling) made acrylonitrile butadiene styrene (ABS) parts," in *ASME International Mechanical Engineering Congress and Exposition*, 2014, p. V011T06A017. https://doi.org/10.1115/IMECE2013-63146
[65] E.F. Abdewi, S. Sulaiman, A.M.S. Hamouda, E. Mahdi, "Quasi-static axial and lateral crushing of radial corrugated composite tubes," *Thin-Walled Structures*, vol. 46, no. 3, pp. 320-332, 2008. https://doi.org/10.1016/j.tws.2007.07.018
[66] B. Zhang, L. Wang, J. Zhang, Y. Jiang, W. Wang, G. Wu, "Deformation and energy absorption properties of cenosphere/aluminum syntactic foam-filled circular tubes under lateral quasi-static compression," *International Journal of Mechanical Sciences*, vol. 192, p. 106126, 2021. https://doi.org/10.1016/j.ijmecsci.2020.106126